Journal of King Saud University - Science 36 (2024) 103042

HOSTED BY

Contents lists available at ScienceDirect

Journal of King Saud University - Science

journal homepage: www.sciencedirect.com

$LnPO_4:Eu^{3+}$ nanoparticles: Role of host lattices on physiochemical and luminescent properties

Anees A Ansari *, M.A. Majeed Khan

College of Sciences, King Saud University, Riyadh 11451, Saudi Arabia

ARTICLE INFO

Keywords:
Metal phosphates
Europium
Crystallographic
Optical bandgap
Luminescent

ABSTRACT

$LnPO_4:Eu^{3+}$ (Ln = La, Gd and Y) nanoparticles (NPs) were prepared at low temperatures via a urea-based thermal decomposition method. X-ray diffraction pattern revealed a hexagonal single phase, high purity with an average crystalline size of 13.9, 14.89, and 18.7 nm for $LaPO_4$:Eu, $GdPO_4$:Eu, and YPO_4:Eu NPs, respectively. Bandgap energies were calculated based on the measure absorption spectra are to be values 5.14, 5.03, and 4.90 eV for the $LaPO_4$:Eu, $GdPO_4$:Eu, and YPO_4:Eu NPs, respectively. A comparative study suggested that the excitation and emission transitions were significantly higher in the $GdPO_4$:Eu NPs and in comparison to the $LaPO_4$:Eu and YPO_4:Eu NPs. It implies the impact of the crystallinity, host lattice, and crystal symmetry, in which doped Eu^{3+}-ion replaces the host cation and distorts the crystal symmetry.

1. Introduction

Currently, luminescent materials are a subject of much interest to researchers because of their usage in a broad range of applications in applied material and biomedical sciences (Ansari et al., 2021, Ansari et al., 2021). Luminescent materials are used in the development of laser diodes, penal displays, photocatalysis, thermometry, optical biosensors, and many more applications (Ren et al., 2020). Till now, a large number of organic dyes, semiconductor materials, and plasmonic nanomaterials have been applied as luminescent materials(Yasin et al., 2023). Because of their weak chemical photo-stability, thermally unstable, photo-bleaching, autofluorescence, short decay time, low biocompatibility, and toxic nature reduced their applicability in clinical trials and other photonic-based applications(Ye et al., 2004, Ansari et al., 2022). These unique characteristics draw the attention of physicists, chemists, and biologists for their future use as per current applications (Ansari et al., 2021, Ansari et al., 2022).

Among the investigated host matrixes oxide-derived nanomaterials were exploited as an important host lattice for the doping of the luminescent Ln^{3+}-ions. Because oxide derived nanomaterials display superior physiochemical properties which differ from their respective metal fluoride host nanomaterials. In particular, metal orthophosphate is a much more explored category of the oxide-derived host matrices, because of their superior thermal (~2300 °C), phonon energy (1100 cm^{-1}), weak solubility, photo-chemical robustness, resistance to photo-bleaching, and minimized phonon energy. Various polymorphism forms of Ln^{3+} orthophosphates exist, including churchite or weinschenkite (monoclinic; naturally frequent), rhabdophane (hexagonal), zircon or xenotime (tetragonal), monazite or monazite (monoclinic), and orthorhombic.

Up to now, various synthesis processes have been described by various researchers for the successful preparation of the $LnPO_4$ NPs(Lai et al., 2009). Among them, the majority of the developed techniques for the preparation of $LnPO_4$ NPs rely on the co-precipitation process. One of the most popular techniques for the synthesis of $LnPO_4$ NPs is co-precipitation (Grzyb et al., 2014). The foundation of this procedure is a chemical exchange relationship that precipitates an insoluble inorganic molecule(Rodriguez-Liviano et al., 2013). The simplicity and low cost of this technology are its main benefits. Additionally, the water-containing reaction environment might cause a substantial amount of water to be soaked on the exterior of the nanocrystal(Parchur et al., 2012). Lai et al. applied a hydrothermal method for the preparation of hexagonal $LaPO_4$:Eu NPs(Lai et al., 2009). Zhang et al used a urea-assisted well-dispersed co-precipitation procedure for the synthesis of uniform YPO_4:Eu hollow spheres(Zhang et al., 2010).

Here, we presented the physiochemical and photoluminescent properties of the optically active $LaPO_4$:Eu, $GdPO_4$:Eu and YPO_4:Eu NPs prepared at low-temperature under a urea-based thermal decomposition

Peer review under responsibility of King Saud University.
* Corresponding author.
E-mail address: aneesahmad@ksu.edu.sa (A.A. Ansari).

https://doi.org/10.1016/j.jksus.2023.103042
Received 16 September 2023; Received in revised form 26 November 2023; Accepted 1 December 2023
Available online 2 December 2023

process. We constant all the synthesis parameters including doping of the activator ion, temperature, solution medium, powder calcination temperature, etc to control the physiochemical characteristics of all three samples. Systematic properties are presented to examine the influence of the host lattice, crystallinity, surface behavior, Raman shift, optical activity, colloidal stability, and photoluminescent (excitation and emission) properties.

2. Experimental

2.1. Materials

La_2O_3(98 %, BDH chemicals, UK), Gd_2O_3(98.8 %, BDH chemicals, England), Yttrium oxide (BDH, chemicals, UK), urea, HNO_3, C_2H_5OH were purchased AR grade and employed as received without further purification. All metal oxides were converted into metal nitrates by dissolving in diluted HNO_3. Milli-Q (Millipore, Bedford, USA) H_2O was utilized for the preparation and characterization of the metal phosphate NPs.

2.2. Synthesis of the Eu^{3+}-ion doped metal phosphate nanoparticles

For the preparation of the $LnPO_4$:Eu NPs, freshly prepared 9.5 ml of 2 M $La(NO_3)_37H_2O$ dissolved in aqueous media, and 0.05 ml 2 M Eu $(NO_3)_36H_2O$ were mixed into 100 ml kept on the hot plate for vigorous mechanical stirring at 70 °C(Phaomei et al., 2010). 5 g urea liquified in an aqueous media was dropwise injected into an ongoing magnetically stirred reaction mixture for slow thermal decomposition of the metal nitrates into metal carbonates. This reaction proceeded on the hot plate until the homogeneous transparent solution occurred. After that, the reaction was transferred into the reflexing condition at an elevated temperature of 150 °C for the complete decay of urea into amine and carbonates. Then an equal volume of NaH_2PO_4 dissolved in an aqueous mixture was dropwise added into the ongoing reaction mixture. This reaction further proceeded for ~ 5 hrs. Occurred precipitate was separated by centrifugation, washed with H_2O to eliminate the unreacted byproducts, and dried overnight in an oven at 80 °C. Similar reaction conditions were employed for the synthesis of $GdPO_4$:Eu and YPO_4:Eu NPs.

2.3. Characterization

Powder XRD pattern (PANalytical X'PERT, Netherland) x-ray diffractometer fitted with Ni filter and Cu Kα (λ = 1.5404 Å) radiation. FTIR spectra Vertex 80 (Bruker, USA) spectrometer was employed using by KBr pellet procedure in 400–4000 cm^{-1} frequency range. Raman spectra were measured from the (IY-Horiba-T64000) Raman spectrometer at ambient temperature under monitoring from 325 nm excitation wavelength. UV/Visible spectra were recorded from the Cary 60 (Agilent Technologies, USA) spectrophotometer in ethanol in the range of 200–650 nm wavelength. Emission and excitation spectra were measured from the Flourolog-3 (Model FL3-11, Horiba Jobin Yvon, Edison, USA) spectrophotometer.

3. Results and discussion

3.1. Crystallographic study

A Powder XRD profile was used to inspect the comparative crystallographic, crystal phase, crystallinity, and phase cleanliness of the as-prepared nano products. As proved in Fig. 1 the diffraction lines' position and intensities in the XRD pattern of the $LaPO_4$:Eu, $GdPO_4$:Eu, and YPO_4:Eu sample were completely matched with the hexagonal structure, which is well-indexed to the JCPDS Card No. 046–1439(Runowski et al., 2014), JCPDS card No. 039–0232(Zhang et al., 2011, Ren et al., 2012) and JCPDS Card No. 042–0082, respectively(Luwang et al., 2010, Lai et al., 2014). No additional peaks related to the metal oxide or other additives are detected in the entire XRD profile, it endorsed the synthesis of a highly pure, one-phase nanoproduct. As presented in Fig. 1**a** the width of the diffraction planes in all three metal phosphate samples was highly broad, it indicated the small crystalline size of the particles. A slight shift in the diffraction peak positions is detected in the YPO_4:Eu NPs than in the $LaPO_4$:Eu and $GdPO_4$:Eu NPs. It assumes that the shifting in the diffraction peaks because of the larger ionic radii Eu^{3+}=0.95 Å doped into the smaller size ionic radii Y^{3+} crystal lattice Y^{3+}=0.89 Å (Fig. 1**b**). It indicated that the substituted Eu^{3+}-ion occupied the Y^{3+} cation positions, therefore the lattice of the crystal was slightly enlarged. The slight enlargement of the host lattice distorts the symmetry because of alterations in the bond angle and bond distances. Causing the symmetry distortion the diffraction plane intensities as well as peak positions were shifted in the XRD pattern (Jia et al., 2010, Yang et al., 2011). Jia et al reported that the ionic radii differences affect the diffraction peak positions in the XRD pattern such as doping of the small size ion into bigger ionic radii host lattice shifts the diffraction peaks at a higher angle, whereas the bigger ionic radii dopant with smaller size ionic radii ions shift the diffraction lines at a lower angle (Y^{3+}=1.019 Å, La^{3+}=1.16 Å, Eu^{3+}=1.06 Å, and Gd^{3+}=1.05 Å in eight coordinated)(Jia et al., 2010). An observed lattice constant are a = 6.798 Å, b = 7.115 Å, and c = 6.591 Å for the $LaPO_4$:Eu; a = 6.708 Å, b = 7.101 Å, and c = 6.482 Å for the $GdPO_4$:Eu; and a = 6.831 Å, b = 6.175 Å, c = 6.652 Å for the YPO_4:Eu NPs. The observed lattice parameters are similar to the previous reports (Parchur et al., 2010, Yaiphaba et al., 2010). A significant reduction in the calculated lattice parameters was observed it

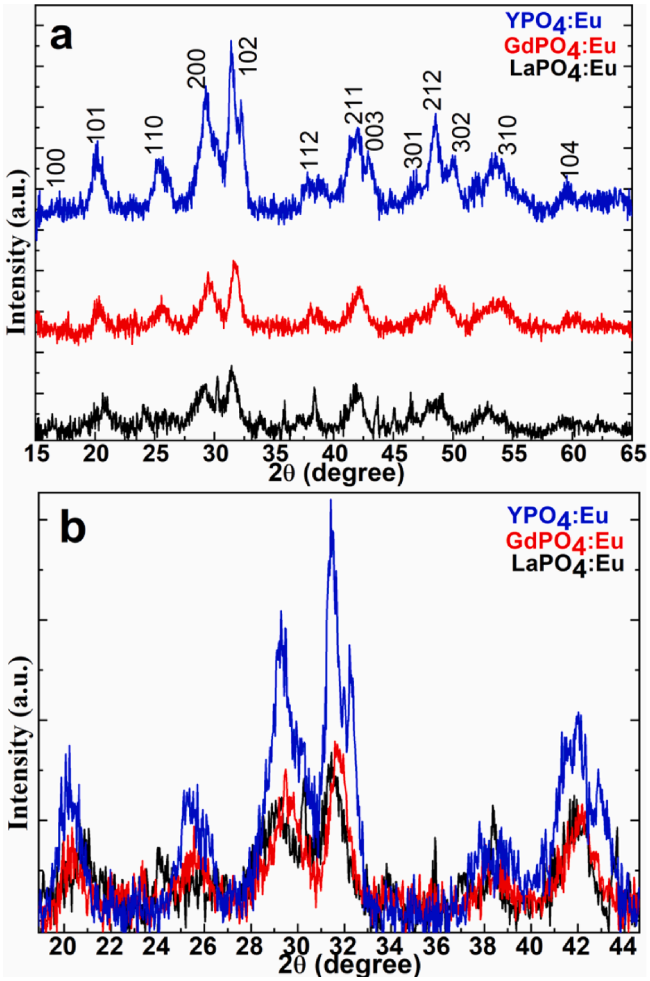

Fig. 1. (a&b)X-ray diffraction pattern of the $LaPO_4$:Eu, $GdPO_4$:Eu, and YPO_4:Eu NPs.

reflects the impact of the variation in the host and doped ions ionic radii (Phaomei et al., 2011). Additionally, the substituted doped ion replaces the host ion causing it to reduce the lattice parameters, which are estimated in the order YPO_4:Eu>$LaPO_4$:Eu> $GdPO_4$:Eu, respectively (Fig. 1) (Grzyb et al., 2014). It is anticipated that in luminescent materials higher crystalline phase typically correlates to fewer trapping agents and brighter fluorescence. In the optically active or photosensitive particle crystal structure, particle size plays an important role in enhancing emission efficiency. A better crystalline phase results in fewer bulk and surface imperfections, which act as photo-induced electron quenching points and reduce luminescence intensity. The average crystalline size of the nanoproducts was assessed from the full-width half maxima of the strongest diffraction plane (1 0 2) observed at 31.7° calculated through the Scherrer equation to be 13.9, 14.89, and 18.7 nm for $LaPO_4$:Eu, $GdPO_4$:Eu, and YPO_4:Eu NPs, respectively.

3.2. Surface properties

FTIR spectra were performed to inspect the attachment of the organic and water molecules surrounding the exterior of the nanocrystals. Fig. 2 displays the FTIR spectra of the as-synthesized $LaPO_4$:Eu, $GdPO_4$:Eu, and YPO_4:Eu NPs in a comparative analysis. All FTIR spectrum shows a diffused band in between 300 and 3600 cm^{-1} attributed to the asymmetric/symmetric stretching vibrational mode of the (O–H) functional group related to the physically or chemically outward adsorbed H_2O particles (Phaomei et al., 2011, Lai et al., 2014). Three strong intensity bands located at ~ 1750, 1250, 640, and 550 cm^{-1} are associated with the asymmetric stretching, bending, and wagging vibrational modes of the phosphate group (PO_4^{3-}) and hydroxyl groups (Ansari, 2017, Ansari et al., 2017). A sharp with a strong middle-intensity peak at a lower frequency appeared at ~ 462 cm^{-1}, which is ascribed to the *meta*-oxygen network (Ansari, 2018, Ansari and Khan, 2018) in the crystal lattice.

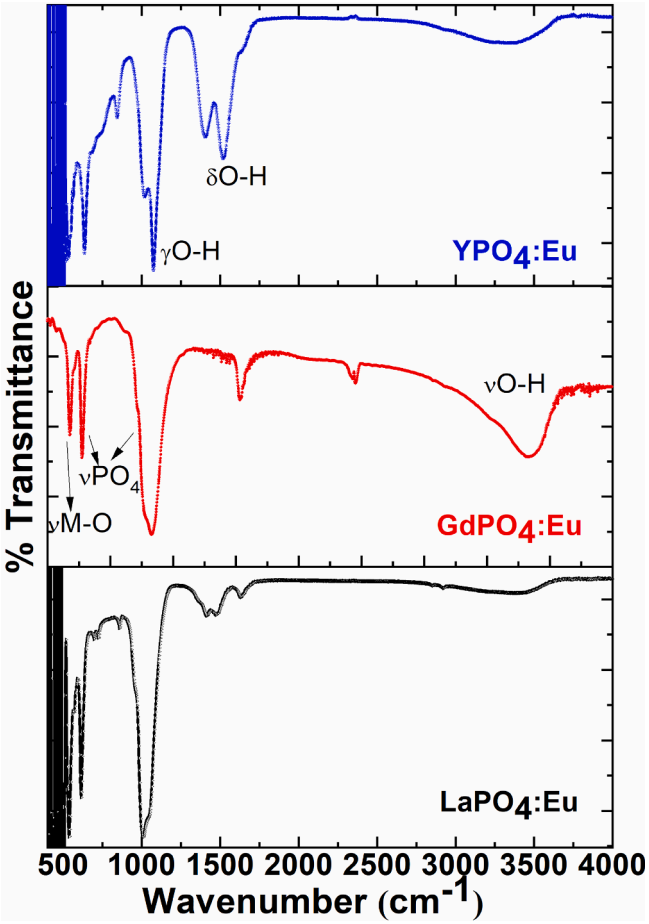

Fig. 2. FTIR spectra of the $LaPO_4$:Eu, $GdPO_4$:Eu, and YPO_4:Eu NPs.

3.3. Raman shift

Raman spectra were recorded to estimate the structural dis-order in three Eu^{3+}-ion doped metal phosphate NPs. Fig. 3 illustrated the comparative Raman spectra of the $LaPO_4$:Eu, $GdPO_4$:Eu, and YPO_4:Eu NPs to distinguish the peak sensitivity and position of the observed Raman vibrational bands(Du et al., 2015, Saraf et al., 2015, Colomer et al., 2017). Raman spectra of the three samples exhibited two strong broadband located at 811, and 880 cm^{-1}, which are credited to the hexagonal phase of the metal phosphates(Colomer et al., 2017). The Raman peak intensity was remarkably higher in the $GdPO_4$:Eu NPs in contrast to the $LaPO_4$:Eu and YPO_4:Eu NPs, it may be the impact of the host and guest ion size, which shrinks/enlarges the crystal lattice-based on the doped cation ionic radii, as described in the XRD discussion.

3.4. Optical characteristics

Fig. 4 displayed the comparative absorption spectra of the as-synthesized Eu^{3+}-ion doped metal phosphate NPs to explore the optical characteristics, aqueous dispersibility, and colloidal solidity in an aqueous solution. The absorption spectra of the $LaPO_4$:Eu, $GdPO_4$Eu, and YPO_4:Eu NPs in an aqueous solution revealed good absorbance in the ultraviolet region. A strong absorbance in the UV range of the as-prepared NPs specified good dispersibility and colloidal stability. It assumes that the exterior of the metal phosphate NPs is shielded with abundant hydroxyl molecules which assist in the formation of hydrogen bonding through van der Waal force interaction (Fig. 4). Generally, it is expected that the high colloidal dispersibility of the NPs leads to an increase in the biocompatibility and non-toxicity of the metal phosphate NPs.

UV/Visible spectra were exploited to monitor the optical energy bandgap (E_g) of the as-prepared three metal phosphate NPs to understand the optical characteristics and their correlation with the grain size of the ceramic materials. Tauc formulae were employed to regulate the bandgap energy, in which absorption spectra were plotted photon energy ($h\nu$) versus $(\alpha h\nu)^2$ as demonstrated in Fig. 5(Tauc and Menth, 1972). According to the curve plotted in Fig. 5, the straight portion of the curve exhibited the indirect E_g values 5.14, 5.03, and 4.90 eV for the $LaPO_4$:Eu, $GdPO_4$:Eu, and YPO_4:Eu NPs, respectively.

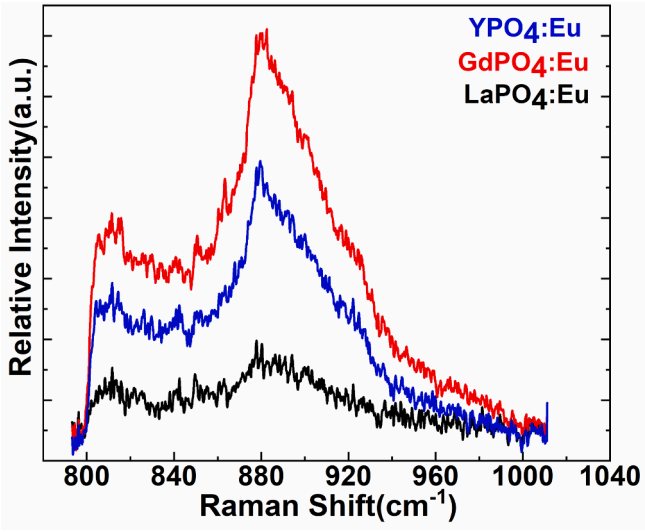

Fig. 3. FT-Raman spectra of the $LaPO_4$:Eu, $GdPO_4$:Eu, and YPO_4:Eu NPs.

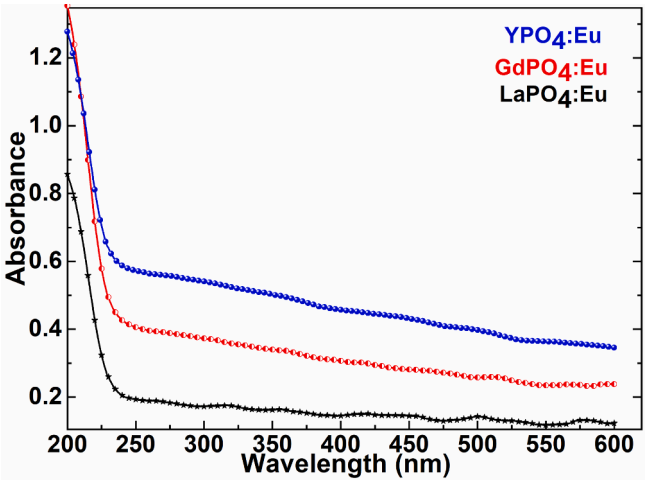

Fig. 4. UV/Visible absorption spectra of the $LaPO_4$:Eu, $GdPO_4$:Eu, and YPO_4:Eu NPs.

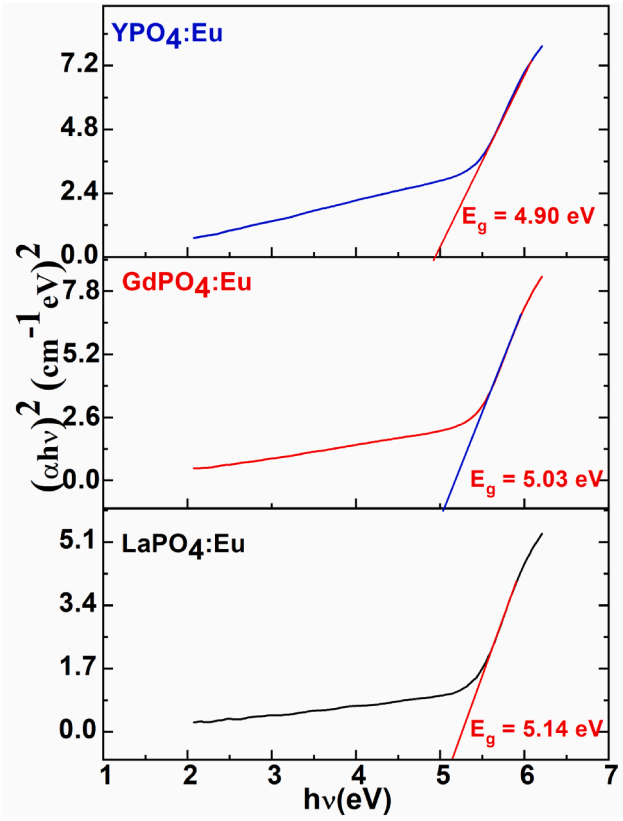

Fig. 5. Energy bandgap plotting a graph between $(\alpha h\nu)^2$ versus photon energy ($h\nu$,eV) of the $LaPO_4$:Eu, $GdPO_4$:Eu, and YPO_4:Eu NPs.

3.5. Photoluminescence properties

Fig. 6 displays the excitation spectrums of the $LaPO_4$:Eu, $GdPO_4$:Eu, and YPO_4:Eu NPs on irradiation of all samples from the 595 nm ($^5D_0 \rightarrow {}^7F_1$) emission wavelength. The excitation spectra of the three-metal phosphate exhibited seven 4f-4f intra-configurational exciton located at 312, 317–324, 363, 375, 393, 437, and 465 nm, which correspond to $^7F_0 \rightarrow {}^5I_6$, $^7F_{0,1} \rightarrow {}^5H_{3,6}$, $^7F_{0,1} \rightarrow {}^5D_4$, $^7F_{0,1} \rightarrow {}^5G_3$, $^7F_{0,1} \rightarrow {}^5L_6$, $^7F_{0,1} \rightarrow {}^5D_3$, and $^7F_{0,1} \rightarrow {}^5D_2$ of the Eu^{3+}-ion, respectively (Fig. 6). An observed intensity in the three metal phosphate NPs is in order $GdPO_4$:Eu>YPO_4:Eu>$LaPO_4$:Eu NPs. As illustrated in Fig. 6 the intensity of the

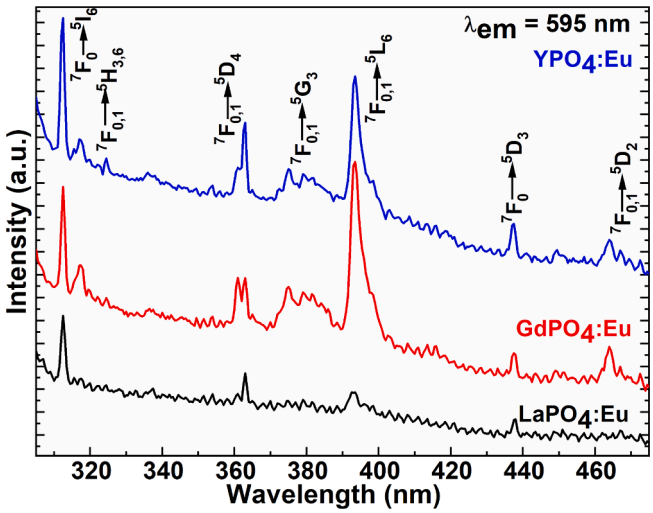

Fig. 6. Excitation spectra of the $LaPO_4$:Eu, $GdPO_4$:Eu, and YPO_4:Eu NPs.

exciton transitions in the case $LaPO_4$:Eu NPs is very weak in contrast to the $GdPO_4$:Eu and YPO_4:Eu NPs. It depends on the charge transfer and crystallinity of the host lattice, which assists in promoting the luminescent efficiency of the doped luminescent center ions.

Emission spectra were monitored under excitation from the $e_x = 393$ nm wavelength in the range from 450 to 750 nm wavelength as shown in Fig. 7**a&b**. The emission spectra in Fig. 7 demonstrated the most intensive luminescence lines located at 467, 534, 590, 612, 644, and 696 nm, which are labeled as $^5D_1 \rightarrow {}^7F_1$, $^5D_1 \rightarrow {}^7F_3$, $^5D_0 \rightarrow {}^7F_1$, $^5D_0 \rightarrow {}^7F_2$, $^5D_0 \rightarrow {}^7F_3$, and $^5D_0 \rightarrow {}^7F_4$, of the 4f-4f intra-configurational Eu^{3+}-ion most emissive transitions, respectively(Ansari, 2017). The emission spectra of the three metal phosphate NPs display the two most intensive emission transitions in the middle of the spectrum, which are assigned as $^5D_0 \rightarrow {}^7F_1$ magnetic-dipole, and $^5D_0 \rightarrow {}^7F_2$ electric-dipole emission lines. The most noticeable emission peak is the so-called hypersensitive red luminescent transition, which is positioned at 612 nm ($^5D_0 \rightarrow {}^7F_2$). The electric dipole ($^5D_0 \rightarrow {}^7F_2$) transition is more robust than the corresponding magnetic-dipole ($^5D_0 \rightarrow {}^7F_1$) transition in the luminescent spectrum if the Eu^{3+}-ion is in a low symmetry location, which indicates it lacks an inversion center(van Hest et al., 2017). However, the position symmetry at which the Eu^{3+}-ion is located does not affect the magnetic dipole ($^5D_0 \rightarrow {}^7F_1$) transition (Yaiphaba et al., 2010). The luminescence spectra of the $GdPO_4$:Eu and YPO_4:Eu NPs illustrated the most sensitive electric dipole ($^5D_0 \rightarrow {}^7F_2$) emission transition(Zhang et al., 2011). In which, magnetic-dipole ($^5D_0 \rightarrow {}^7F_1$) emission transition is less sensitive as exhibited in Fig. 7**a&b**. It implies that the doped Eu^{3+}-ion in the $GdPO_4$ and YPO_4 crystal matrix is present in the asymmetric position in both host materials(Zhang et al., 2010, Sahu et al., 2012).

Although in the case of $LaPO_4$:Eu NPs magnetic-dipole and electric-dipole, both transitions showed equal sensitivity, even though the efficiency of the magnetic-dipole emission transition is slightly greater in comparison to the electric-dipole transition, it endorsed that the Eu^{3+}-ion exists in the host lattice in inversion symmetry with C_1 space group. These results are quite similar to the previous reports (Buissette et al., 2004, Lai et al., 2009). Rambabu et al. described that the enhancement in the magnetic-dipole ($^5D_0 \rightarrow {}^7F_1$) emission peak in contrast to the electric-dipole ($^5D_0 \rightarrow {}^7F_2$) emission peak caused the easy charge transfer between the host and doped cations(Rambabu and Buddhudu, 2001). Similar observations were reported by Yu et al., an alteration in the emission intensity of the two most sensitive luminescence transitions of Eu^{3+}-ion(Yu et al., 2004). Despite low-temperature preparation, the primary Eu^{3+} positions symmetry is similar to that of the macro-size - material(Ferhi et al., 2009). As exhibited in Fig. 7 the intensity ratio of the emission transitions indicated that a large number of Eu^{3+} ions inhibit the inversion position in the $LaPO_4$:Eu NPs(Phaomei et al.,

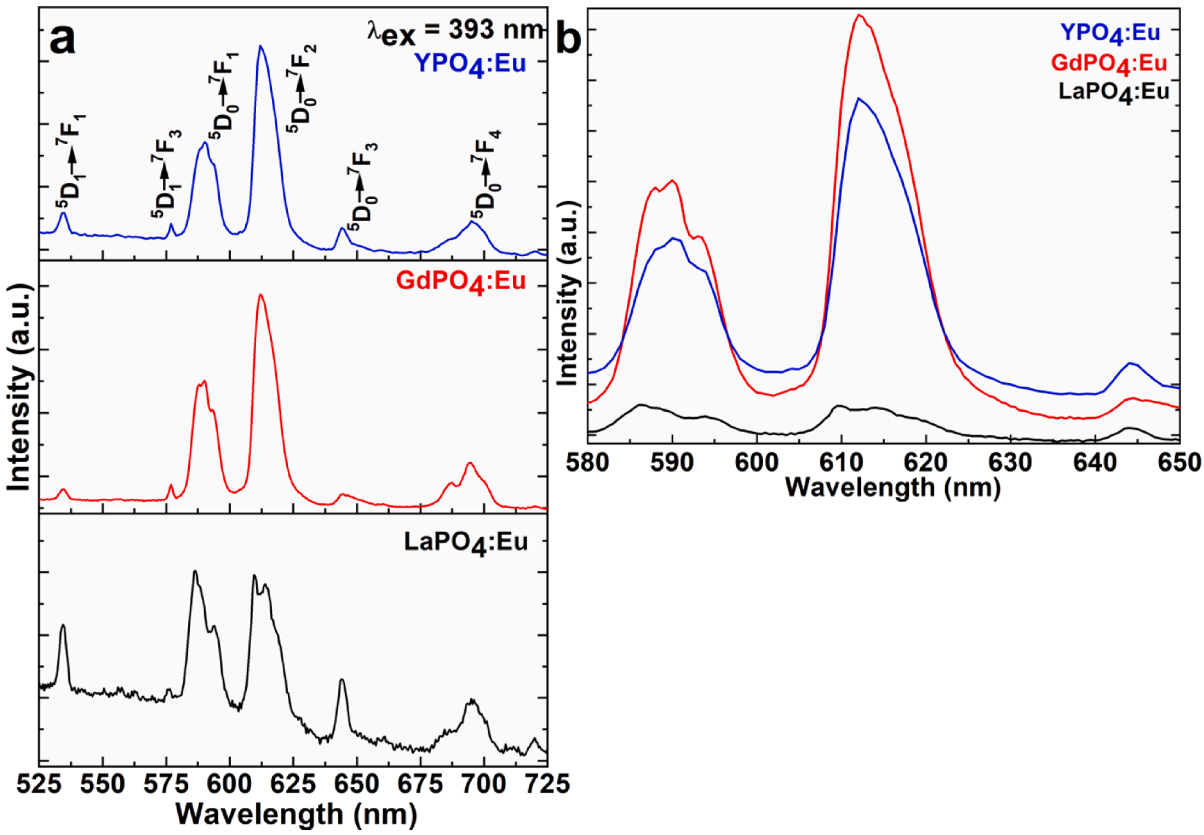

Fig. 7. (a&b) Emission spectra of the $LaPO_4$:Eu, $GdPO_4$:Eu, and YPO_4:Eu NPs.

2010). The host lattice diameter, shape, crystal phase, and lattice locations for Eu^{3+} ions are significant variables that significantly distress luminescent efficiency. The La^{3+} site that exhibits C_1 point group symmetry in the monoclinic crystal structure of $LaPO_4$ has non-inversion symmetry(Lai et al., 2009, Phaomei et al., 2010).

It is a fact that due to small atomic size differences, Eu^{3+} ions (1.06 Å) and La^{3+} ions (1.16 Å) can both occupy the same locations in a crystal. The emission efficacy of the materials is greatly influenced by the excellent crystallinity and crystal shape of the ceramic materials (Phaomei et al., 2010). It is a proven fact that good crystalline structure constantly favors increasing emission and excitation efficiency. Small grains and a large surface area allow for easy H_2O molecule adsorption on their exterior, which also allows for the coordination of organic moieties. Considering that metal phosphate NPs are made in an aqueous solvent and that hydroxyl groups may be present on their surface, these findings are also supported by the observed FTIR spectral results. Surfaces adsorbed high vibrational energy either H_2O or other organic functional group molecules quenched the luminescence intensity owing to the non-radiative recombination trap molecules that are accountable for suppressing the emission efficiency of the materials. As observed in Fig. 7, the emission spectra display a feeble intensity of the emission transition situated at ~ 534 nm corresponds to the ($^5D_1 \rightarrow {}^7F_1$) transition, which seems caused by the $LnPO_4$ host lattice's low vibrational energy (350 cm^{-1}). This finding suggests that the host material protects the Eu^{3+} ion from the nearby H_2O molecules, because high phonon energy (3500 cm^{-1}) molecules, effectively quenched the emission efficiency of the doped luminescent ion.

In a comparative spectral study, the emission transitions in the $GdPO_4$:Eu NPs are significantly highly sensitive in comparison to the YPO_4:Eu and $LaPO_4$:Eu NPs(Lai et al., 2014). It is a fact that the Gd^{3+} ion displays strong absorption transition located at ~ 250, and 270 nm assigned to $^8S \rightarrow {}^6D$ and $^8S_{7/2} \rightarrow {}^6I_j$ transitions overlap on the $^5D_0$ level of the Eu^{3+} ion as appeared in the luminescent spectrums, that effectively charge transfer from Gd^{3+}-ion to the doped Eu^{3+}-ion leading to enhance the emission efficiency, similar observations also reported in a previous report(Fig. 7**b**) (Buissette et al., 2004, Rodriguez-Liviano et al., 2013). Because yttrium and lanthanum both are diamagnetic because their 4d subshell is filled and the absence of the 4f-subshell. However, the observed emission spectral results suggested that the $LaPO_4$ is not a suitable host for doping of the Eu^{3+}-ion in comparison to the $GdPO_4$ and YPO_4 host lattice. However, the emission and excitation findings suggested that the $GdPO_4$:Eu^{3+} is the best host matrix for producing excellent emission efficiency.

4. Conclusion

Eu^{3+}-doped metal phosphate NPs were synthesized to examine the effect of the host lattice on physiochemical, and luminescent characteristics. The sensitivity of the diffraction peaks, peak positions, lattice parameters, and crystallinity confirmed that the doping of the luminescent Eu^{3+}-ion disturbed the crystal symmetry, because of the difference between the host and doped cation ionic radii. FTIR spectra verified the presence of the phosphate group and hydroxyl group IR vibrational bands. Raman shift and bandgap energy reflected the presence of Raman active modes and optical activity in the UV/visible region. The emission and excitation transitions were dominant in the order $GdPO_4$:Eu > YPO_4:Eu > $LaPO_4$:Eu NPs, respectively. The high sensitivity of the excitation and emission transitions in the $GdPO_4$:Eu NPs because of the easy charge transfer process between the Gd^{3+}-ion and Eu^{3+}-ion. However, the sensitivity of the magnetically-dipole transition and electric-dipole transition were highly affected in all three metal phosphate samples in comparison to the conversational metal oxide host lattices. Based on the observed results, $GdPO_4$:Eu NPs are highly useful in luminescent-based biotechnological applications.

Declaration of competing interest

The authors declare that they have no known competing financial interests or personal relationships that could have appeared to influence the work reported in this paper.

Acknowledgment

The author is thankful to the Researchers Supporting Project number (RSP2023R365), King Saud University, Riyadh, Saudi Arabia.

Appendix A. Supplementary material

Supplementary data to this article can be found online at https://doi.org/10.1016/j.jksus.2023.103042.

References

Ansari, A.A., 2017. Photochemical studies of monodispersed YPO4: Eu microspheres: The role of surface modification on structural and luminescence properties. J. Photoch. Photobio. A 343, 126–132. https://doi.org/10.1016/j.jphotochem.2017.04.021.

Ansari, A.A., 2018. Silica-modified luminescent LaPO4:Eu@LaPO4@SiO2 core/shell nanorods: Synthesis, structural and luminescent properties. Luminescence 33 (1), 112–118. https://doi.org/10.1002/bio.3379.

Ansari, A.A., Khan, M.A.M., 2018. Structural and spectroscopic studies of LaPO4:Ce/Tb@LaPO4@SiO2 nanorods: Synthesis and role of surface coating. Vib. Spectrosc. 94, 43–48. https://doi.org/10.1016/j.vibspec.2017.12.001.

Ansari, A.A., Labis, J.P., Manthrammel, M.A., 2017. Designing of luminescent GdPO4: Eu@LaPO4@SiO2 core/shell nanorods: Synthesis, structural and luminescence properties. Solid State Sci. 71, 117–122. https://doi.org/10.1016/j.solidstatesciences.2017.07.012.

Ansari, A.A., Parchur, A.K., Thorat, N.D., et al., 2021. New advances in pre-clinical diagnostic imaging perspectives of functionalized upconversion nanoparticle-based nanomedicine. Coord. Chem. Rev. 440, 213971 https://doi.org/10.1016/j.ccr.2021.213971.

Ansari, A.A., Thakur, V.K., Chen, G., 2021. Functionalized upconversion nanoparticles: New strategy towards FRET-based luminescence bio-sensing. Coord. Chem. Rev. 436, 213821 https://doi.org/10.1016/j.ccr.2021.213821.

Ansari, A.A., Muthumareeswaran, M.R., Lv, R., 2022. Coordination chemistry of the host matrices with dopant luminescent Ln3+ ion and their impact on luminescent properties. Coordin. Chem. Rev. 466, 214584 https://doi.org/10.1016/j.ccr.2022.214584.

Ansari, A.A., Parchur, A.K., Chen, G., 2022. Surface modified lanthanide upconversion nanoparticles for drug delivery, cellular uptake mechanism, and current challenges in NIR-driven therapies. Coord. Chem. Rev. 457, 214423 https://doi.org/10.1016/j.ccr.2022.214423.

Buissette, V., Moreau, M., Gacoin, T., et al., 2004. Colloidal synthesis of luminescent rhabdophane LaPO4: Ln(3+)center dot xH(2)O (Ln = Ce, Tb, Eu; x approximate to 0.7) nanocrystals. Chem. Mater. 16 (19), 3767–3773. https://doi.org/10.1021/cm049323a.

Colomer, M.T., Bartolomé, J., Ortiz, A.L., et al., 2017. Raman characterization and photoluminescence properties of La1-xTbxPO4·nH2O and La1-xTbxPO4 phosphor nanorods prepared by microwave-assisted hydrothermal synthesis. Ceram. Int. 43 (14), 10840–10847. https://doi.org/10.1016/j.ceramint.2017.05.110.

Du, Q.J., Huang, Z.B., Wu, Z., et al., 2015. Facile preparation and bifunctional imaging of Eu-doped GdPO4 nanorods with MRI and cellular luminescence. Dalton T. 44 (9), 3934–3940. https://doi.org/10.1039/c4dt03444a.

Ferhi, M., Horchani-Naifer, K., Ferid, M., 2009. Combustion synthesis and luminescence properties of LaPO4: Eu (5%). J. Rare Earth 27 (2), 182–186. https://doi.org/10.1016/S1002-0721(08)60216-1.

Grzyb, T., Wiglusz, R.J., Gruszeczka, A., et al., 2014. Down- and up-converting dual-mode YPO4:Yb3+, Tb3+ nanocrystals: synthesis and spectroscopic properties. Dalton T. 43 (46), 17255–17264. https://doi.org/10.1039/c4dt02234c.

Jia, G.A., You, H.P., Song, Y.H., et al., 2010. Facile synthesis and luminescence of uniform Y2O3 hollow spheres by a sacrificial template route. Inorg. Chem. 49 (17), 7721–7725. https://doi.org/10.1021/ic100430g.

Lai, H., Bao, A., Yang, Y.M., et al., 2009. Selective synthesis and luminescence property of monazite- and hexagonal-type LaPO4: Eu nanocrystals. CrstEngComm 11 (6), 1109–1113. https://doi.org/10.1039/b818877g.

Lai, H., Du, Y., Zhao, M., et al., 2014. Effects of different organic additives on the formation of YPO4:Eu3+ nano-/microstructures under hydrothermal conditions with enhanced photoluminescence. Ceram. Int. 40 (1), 1885–1891. https://doi.org/10.1016/j.ceramint.2013.07.094.

Luwang, M. N., R. S. Ningthoujam, Jagannath, et al., 2010. Effects of Ce3+ Codoping and Annealing on Phase Transformation and Luminescence of Eu3+-Doped YPO4 Nanorods: D2O Solvent Effect. J Am Chem Soc. 132 (8) 2759-2768. 10.1021/ja909578s.

Parchur, A. K., G. S. Okram, R. A. Singh, et al., 2010. Effect Of EDTA On Luminescence Property Of Eu+3 Doped YPO4 Nanoparticles. International Conference on Physics of Emerging Functional Materials (Pefm-2010). 1313 391-+.

Parchur, A.K., Prasad, A.I., Rai, S.B., et al., 2012. Improvement of blue, white and NIR emissions in YPO4:Dy3+ nanoparticles on co-doping of Li+ ions. Dalton T. 41 (45), 13810–13814. https://doi.org/10.1039/c2dt32062b.

Phaomei, G., Ningthoujam, R.S., Singh, W.R., et al., 2010. Low temperature synthesis and luminescence properties of re-dispersible Eu3+ doped LaPO4 nanorods by ethylene glycol route. Opt. Mater. 32 (5), 616–622. https://doi.org/10.1016/j.optmat.2009.12.009.

Phaomei, G., Ningthoujam, R.S., Singh, W.R., et al., 2011. Luminescence switching behavior through redox reaction in Ce3+ co-doped LaPO4:Tb3+ nanorods: Re-dispersible and polymer film. Dalton T. 40 (43), 11571–11580. https://doi.org/10.1039/c1dt11264c.

Phaomei, G., Singh, W.R., Ningthoujam, R.S., 2011. Solvent effect in monoclinic to hexagonal phase transformation in LaPO4:RE (RE=Dy3+, Sm3+) nanoparticles: Photoluminescence study. J. Lumin. 131 (6), 1164–1171. https://doi.org/10.1016/j.jlumin.2011.02.023.

Rambabu, U., Buddhudu, S., 2001. Optical properties of LnPO4:Eu3+ (Ln=Y, La and Gd) powder phosphors. Opt. Mater. 17 (3), 401–408. https://doi.org/10.1016/S0925-3467(00)00103-8.

Ren, W., Lin, G., Clarke, C., et al., 2020. Optical nanomaterials and enabling technologies for high-security-level anticounterfeiting. Adv. Mater. 32 (18), 1901430. https://doi.org/10.1002/adma.201901430.

Ren, W.L., Tian, G., Zhou, L.J., et al., 2012. Lanthanide ion-doped GdPO4 nanorods with dual-modal bio-optical and magnetic resonance imaging properties. Nanoscale 4 (12), 3754–3760. https://doi.org/10.1039/c2nr30683b.

Rodriguez-Liviano, S., Becerro, A.I., Alcantara, D., et al., 2013. Synthesis and properties of multifunctional tetragonal Eu:GdPO4 nanocubes for optical and magnetic resonance imaging applications. Inorg. Chem. 52 (2), 647–654. https://doi.org/10.1021/ic3016996.

Runowski, M., Grzyb, T., Zep, A., et al., 2014. Eu3+ and Tb3+ doped LaPO4 nanorods, modified with a luminescent organic compound, exhibiting tunable multicolour emission. Rsc Adv. 4 (86), 46305–46312. https://doi.org/10.1039/c4ra06168c.

Sahu, N. K., R. S. Ningthoujam and D. Bahadur, 2012. Disappearance and recovery of luminescence in GdPO4:Eu3+ nanorods: Propose to water/OH center dot release under near infrared and gamma irradiations. J Appl Phys. 112 (1) Artn 014306 10.1063/1.4731644.

Saraf, M., Kumar, P., Kedawat, G., et al., 2015. Probing highly luminescent europium-doped lanthanum orthophosphate nanorods for strategic applications. Inorg. Chem. 54 (6), 2616–2625. https://doi.org/10.1021/ic5027784.

Tauc, J., Menth, A., 1972. States in the gap. J. Non-Cryst. Solids 8–10, 569–585. https://doi.org/10.1016/0022-3093(72)90194-9.

van Hest, J.J.H.A., Blab, G.A., Gerritsen, H.C., et al., 2017. Probing the influence of disorder on lanthanide luminescence using Eu-doped LaPO4 nanoparticles. J. Phys. Chem. C 121 (35), 19373–19382. https://doi.org/10.1021/acs.jpcc.7b06549.

Yaiphaba, N., R. S. Ningthoujam, N. S. Singh, et al., 2010. Luminescence, lifetime, and quantum yield studies of redispersible Eu3+-doped GdPO4 crystalline nanoneedles: Core-shell and concentration effects. J Appl Phys. 107 (3) Artn 034301 10.1063/1.3294964.

Yang, P.P., Gai, S.L., Liu, Y.C., et al., 2011. Uniform hollow Lu2O3: Ln (Ln = Eu3+, Tb3+) spheres: Facile synthesis and luminescent properties. Inorg. Chem. 50 (6), 2182–2190. https://doi.org/10.1021/ic101605k.

Yasin, G., Ali, S., Ibraheem, S., et al., 2023. Simultaneously engineering the synergistic-effects and coordination-environment of dual-single-atomic iron/cobalt-sites as a bifunctional oxygen electrocatalyst for rechargeable zinc-air batteries. ACS Catal. 13 (4), 2313–2325. https://doi.org/10.1021/acscatal.2c05654.

Ye, Z.Q., Tan, M.Q., Wang, G.L., et al., 2004. Novel fluorescent europium chelate-doped silica nanoparticles: preparation, characterization and time-resolved fluorometric application. J. Mater. Chem. 14 (5), 851–856. https://doi.org/10.1039/b311905j.

Yu, L., Song, H., Lu, S., et al., 2004. Luminescent properties of LaPO4: Eu nanoparticles and nanowires. J. Phys. Chem. B 108 (43), 16697–16702. https://doi.org/10.1021/jp047688c.

Zhang, L.H., Jia, G., You, H.P., et al., 2010. Sacrificial template method for fabrication of submicrometer-sized YPO4:Eu3+ hierarchical hollow spheres. Inorg. Chem. 49 (7), 3305–3309. https://doi.org/10.1021/ic9022739.

Zhang, L.H., Yin, M.L., You, H.P., et al., 2011. Mutifuntional GdPO4:Eu3+ hollow spheres: Synthesis and magnetic and luminescent properties. Inorg. Chem. 50 (21), 10608–10613. https://doi.org/10.1021/ic200867a.